cosmetics

MDPI

Article

Protective Effects of Antioxidant Chaga Mushroom Decoction on Normal Human Dermal Fibroblasts Exposed to UV-A

Naoki Doi [1,*], Sayaka Eiyama [1], Kazuichi Araki [2], Kyosuke Miyagawa [1], Ayaka Koike [1], Yukinori Yamauchi [3], Shin-ichi Kondo [1] and Masayuki Kuzuya [1,†]

[1] Laboratory of Pharmaceutical Physical Chemistry, Gifu Pharmaceutical University, 1-25-4, Daigaku-nishi, Gifu 501-1196, Japan; 205017@gifu-pu.ac.jp (S.E.); 215112@gifu-pu.ac.jp (K.M.); 215045@gifu-pu.ac.jp (A.K.); skondo@gifu-pu.ac.jp (S.-i.K.); code.doi0620@gmail.com (M.K.)
[2] Be GLAD Ichiyo Co., Ltd., 13-1 Okucho-Shimokawada, Ichinomiya 491-0201, Aichi, Japan; zenmo19870620@yahoo.co.jp
[3] Department of Pharmaceutical Physical Chemistry, College of Pharmaceutical Sciences, Matsuyama University, 4-2 Bunkyo-cho, Matsuyama 790-8578, Ehime, Japan; yyamauch@g.matsuyama-u.ac.jp
* Correspondence: doi@gifu-pu.ac.jp; Tel.: +81-58-230-8100
† Deceased author.

Abstract

Skin cells exposed to ultraviolet (UV) radiation may experience reduced elasticity in skin tissue due to the production of reactive oxygen species (ROS) and the overexpression of collagen type I-degrading enzymes (MMP-1). Beyond preventing UV exposure with sunscreen, components that protect the inner surface of skin tissue may suppress the expression of ROS and their subsequent effects. In this study, the suppression of ROS production from UV-A-irradiated normal human dermal fibroblasts (NHDFs) using Chaga-derived polyphenol decoction (CPD) was examined with confocal laser scanning microscopy. Pretreatment with CPD reduced ROS expression to less than 5% compared to the blank. The evaluation of MMP-1 expression levels induced by ROS production from UV-A-irradiated NHDFs using an ELISA showed that MMP-1 expression in CPD-pretreated NHDFs was suppressed by more than 30% compared to untreated NHDFs. Furthermore, three-dimensional collagen gels containing NHDFs were prepared, and a dynamic mechanical analysis of the elasticity of UV-A-irradiated gels revealed that pretreatment with CPD maintained elasticity at more than five times that of the CPD-untreated gel. These findings suggest that CPD may be promising as a functional food for protecting skin tissue.

Keywords: Chaga; polyphenol; antioxidant; UV-A; collagen; MMP-1

Check for updates

Academic Editor: Bryan Fuller

Received: 6 March 2026
Revised: 13 June 2026
Accepted: 23 June 2026
Published: 29 June 2026

Copyright: © 2026 by the authors. Licensee MDPI, Basel, Switzerland. This article is an open access article distributed under the terms and conditions of the Creative Commons Attribution (CC BY) license.

1. Introduction

Improving quality of life (QOL) is important for humans to live healthier lives. Consuming foods and supplements that contribute to beauty and health can improve QOL and skin condition and may change people's lives significantly. Human skin is composed of three layers, namely, the epidermis, the dermis, and the subcutaneous tissue, with the dermis making up the majority of the skin. Approximately 70% of the dermis is composed of collagen, and 5% consists of fibrous proteins such as elastin. These proteins are involved in forming the skin's shape, elasticity, and firmness [1,2]. Furthermore, the spaces between these proteins are filled with a gelatinous matrix such as hyaluronic acid, a type of polysaccharide. Hyaluronic acid has the ability to retain water molecules and moisturize the skin [3,4]. These proteins and polysaccharides are produced by skin fibroblasts in the dermis and serve as important factors for maintaining healthy skin.

The skin is an important organ providing protection from harmful environmental stimuli, but it can be susceptible to deterioration due to intrinsic factors (e.g., age and genetics) and extrinsic factors (e.g., ultraviolet rays, environmental pollution, chemicals, and smoking). The influence of UV rays on the skin has been reported, and it is estimated that 90% of skin aging may be caused by UV exposure [5–7]. There are two types of UV rays reaching the Earth from the sun. UV-A rays, which have a long wavelength (320~400 nm) and account for approximately 95% of UV rays, can penetrate into the dermis and induce suntan, indicating skin darkening associated with melanin. Reactive oxygen species (ROS) are also produced in normal human dermal fibroblasts (NHDFs) exposed to UV-A. The generated ROS may also induce the overexpression of mRNA and subsequently produce collagenase, such as matrix metalloproteinase-1 (MMP-1), which can decompose the collagen in the skin [8,9]. The reduction in collagen in the skin leads to the formation of deep wrinkles and sagging. Therefore, antioxidant compounds that inhibit the production of ROS in NHDFs are useful for suppressing the degradation of collagen in the skin.

Chaga mushroom (*Inonotus obliquus*) is a white-rot fungus belonging to the Hymenochaetaceae family of basidiomycetes, which grows on birch trees in northern climates such as Russia [10]. Chaga mushroom has traditionally been used to treat various diseases in Russia, Western Siberia, Asia, and North America [11]. It has been reported that Chaga mushroom has various biological activities, such as anti-inflammatory [12], immunomodulatory [13], anti-viral [14], anti-fatigue [15], and antioxidant effects [16,17]. These activities are induced by bioactive compounds, such as β-glucan, triterpenoids, and polyphenols (e.g., gallic acid, protocatechuic acid, 3,4-dihydroxybenzenzaldehyde, caffeic acid, and syringic acid) from Chaga mushroom [18–20]. Chaga mushrooms grown in extremely cold regions may have these bioactive compounds in high amounts to protect themselves from environmental stress. The total phenolic content of Chaga mushroom is 166 mg of gallic acid equivalent/g [18], whereas that of edible mushrooms *Ganoderma lucidum* and *Lentinula edodes* is 16.4 mg/g and 7.25 mg/g [21]. Therefore, Chaga mushroom is promising as a strong antioxidant. The components of Chaga mushroom have often been extracted with organic solvents, since cross-linked chitin, β-glucans, and other components are hydrophobic and contained within rigid cell walls [18]. Our research group recently reported the anti-glycation and antioxidant effects of Chaga polyphenol decoction (CPD) extracted from Chaga mushroom with water [22]. CPD exhibited 3~4 times higher anti-glycation activity on serum albumin and collagen gels than the standard anti-glycation agent, 2-aminoguanidine. It was also revealed that CPD efficiently scavenged the ROS produced in human skin fibroblasts exposed to UV-A. However, the specific localization and the amount of ROS expression in human skin fibroblasts have not yet been elucidated. Furthermore, it is important to clarify the extent to which CPD's antioxidant effects in human skin fibroblasts depend on concentration and time course.

This study aimed to reveal the antioxidant activity of CPD on NHDFs exposed to UV-A, as shown in Figure 1. The localization and the amount of ROS produced in NHDFs exposed to UV-A were examined with confocal laser scanning microscopy (CLSM), and the required dosage of CPD for antioxidant activity in NHDFs was determined. In addition, the expression levels of MMP-1 produced in NHDFs exposed to UV-A and the inhibitory effects of CPD were evaluated by ELISA. Furthermore, a three-dimensional collagen gel containing NHDFs was prepared, and the ability of CPD to suppress the degradation of collagen gel elastic properties induced by UV-A irradiation was verified.

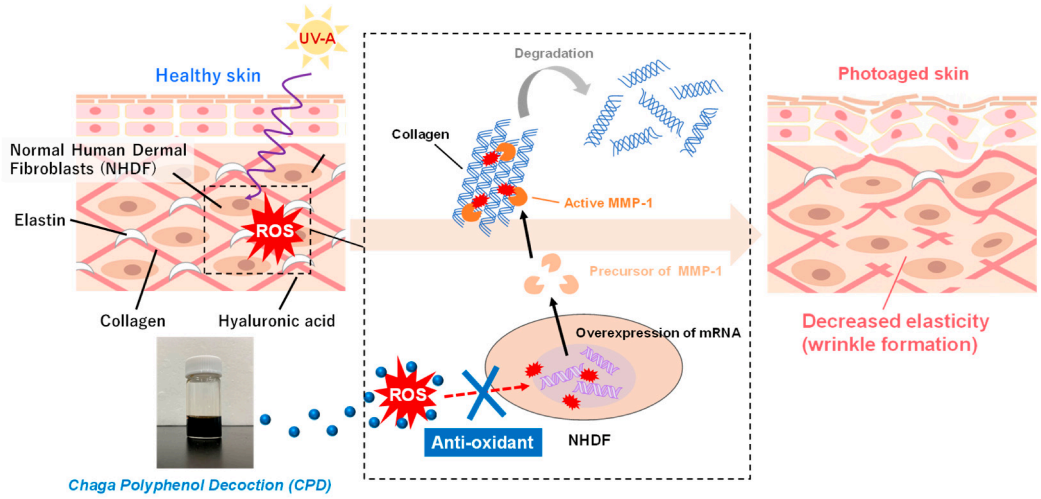


Figure 1. Schematic diagram of this study. CPD suppressed MMP-1 expression and the reduction in collagen gel elasticity in UV-A-exposed NHDFs through its antioxidant effects.

2. Materials and Methods

2.1. Preparation of Chaga Polyphenol Decoction (CPD)

CPD, which was similar to that used in a previous study [22], was prepared by Be GLAD Ichiyo Co., Ltd. Briefly, lactic acid bacteria (*Lactobacillus* and *Bacillus subtilis*) were added at 3% (*v*/*v*) to an aqueous medium containing approximately 65% (*w*/*v*) plant-derived starch (corn cob, coffee, tofu meal, crushed bamboo, and grass), and the medium was fermented at room temperature for 1 month. Each mushroom fungus (shiitake, enokitake, maitake, shimeji, and king trumpet mushroom) was added to the fermentation medium at 3% (*v*/*v*), and fermentation was continued at room temperature for 3 months. Chaga mushroom collected in the Irkutsk region of Russia was extracted under optimal extraction conditions using the prepared fermentation medium. Crushed dry Chaga mushroom was added to the fermentation medium at 20% (*w*/*v*), and then the solution was boiled for 24 h at 100 °C. The resulting CPD was cooled to room temperature and filtered.

2.2. HPLC and Size Exclusion Chromatography (SEC) Measurements

The components in CPD were evaluated by HPLC using the following equipment and parameters: a Hewlett-Packard HPLC system (Hewlett-Packard, Agilent 1100, Palo Alto, CA, USA) equipped with an Agilent 1100 Series autosampler and Hewlett-Packard Agilent 1100 data analysis software (Agilent Technologies, Santa Clara, CA, USA); an excitation wavelength of 200 nm; a binary phase in an InertSustain C18 analytical column (particle diameter of 5 µm, 4.6 × 250 mm) (GL sciences Inc., Tokyo, Japan); a mobile phase comprising acetonitrile/water (60:40, *v*/*v*%); a flow rate of 1.0 mL min^{-1}; an injection volume of 10 µL; and a column temperature of 40 °C.

The molecular weights of the resulting polymers in CPD were determined by SEC at 40 °C (flow rate: 0.7 mL min^{-1}) in pH 7.4 phosphate-buffered saline (PBS) containing 100 mM NaCl as an eluent. Three kinds of polyvinylalcohol gel columns (Asahipak GF-1G 7B: particle size = 9 µm; 7.5 i.d. × 50 mm; Asahipak GS-320 HQ: exclusion limit = 4.0 × 10^4, particle size = 5 µm; 7.5 i.d. × 300 mm; and Asahipak 7M-HQ: exclusion limit = 1.0 × 10^8; particle size = 9 µm; 7.5 i.d. × 300 mm) were connected to a PU 880 high-performance liquid chromatography (HPLC) unit (GL Sciences Inc., Tokyo, Japan) equipped with a RI-2000 refractive index detector (Lab system Co., Ltd., Tokyo, Japan), a model 554 LC column oven (GL Sciences Inc., Japan), and a data analyzer (Runtime Instruments Chromato-PRO, Runtime Instruments Ltd., Tokyo,

Japan). The system was calibrated with pullulan standards (Shodex; peak molecular weight (M_p) = 5900, 9600, 21,100, 47,100, 107,000, 194,000, 337,000, and 642,000 g mol^{-1}).

2.3. Folin–Ciocalteu Method for Determination of Polyphenol Concentration

The polyphenol concentration of each compound was determined using the Folin–Ciocalteu method [23–25]. Briefly, 10% (*v*/*v*) phenol reagent was prepared by diluting 2 mL of phenol reagent (Nacalai Tesque Inc., Kyoto, Japan) to 20 mL with distilled water. A 7.5% (*w*/*v*) sodium carbonate aqueous solution was also prepared by dissolving 3.75 g of sodium carbonate (Nacalai Tesque Inc., Kyoto, Japan) in 50 mL of distilled water. Then, 100 mg of gallic acid anhydrous (Tokyo Chemical Industry Co., Ltd., Tokyo, Japan) was dissolved in 100 mL of distilled water, and the resulting aqueous solution was serially diluted. Then, 10 µL of each aqueous solution (gallic acid, CPD, caffeic acid from Tokyo Chemical Industry Co., Ltd. (Tokyo, Japan), and lignin from Tokyo Chemical Industry Co., Ltd. (Tokyo, Japan)) prepared at various concentrations was dispensed into each well of a 96-well plate. Then, 50 µL of 10% (*v*/*v*) phenol reagent was added to each well, and the plates were shaken for 5 min at room temperature in the dark. After adding 40 µL of a 7.5% (*w*/*v*) sodium carbonate aqueous solution to the mixture, the plates were left to stand for 1 h at room temperature in the dark, and the absorbance of each well at 600 nm was measured with a GloMax® Discover/Explorer System (Promega Corp., Madison, WI, USA). The polyphenol concentration of each sample was calculated by converting the concentration of gallic acid based on the calibration curve for each sample, using Equation (1).

$$\text{Polyphenol concentration expressed as gallic acid } (\mu g/mL) = (S_{sam} - Int_{gal}) / S_{gal}, \quad (1)$$

where S_{sam}, $Int_{gal,}$ and S_{gal} are the slope of the sample, the intercept of gallic acid, and the slope of gallic acid, respectively.

2.4. Antioxidant Assay with 1,1-Diphenyl-2-picryl-hydrazyl (DPPH)

The radical scavenging effect of each antioxidant was confirmed by ESR measurements using DPPH as a stable free radical [26–28]. Briefly, 1.97 mg of DPPH was dissolved in ethanol (EtOH) to prepare 10 mL of 0.5 mM DPPH solution. Then, 4 mg of lignin was dissolved in a mixture of 1 mL of 0.5 M NaOH aqueous solution and 9 mL of EtOH, filtered through a membrane filter (0.45 µm, TORAST™ Disc, Shimadzu GLC Ltd., Tokyo, Japan), and the resulting filtrate was neutralized with a 1 M HCl aqueous solution. The solution was then diluted with EtOH to prepare lignin sample solutions of various concentrations. A total of 2 mg of caffeic acid was also dissolved in a mixture of 1 mL of 0.5 M NaOH aqueous solution and 9 mL of EtOH, filtered through a 0.45 µm filter, and the resulting filtrate was neutralized using 1 M HCl aqueous solution. The caffeic acid sample solutions at various concentrations were prepared by diluting with EtOH. CPD was then diluted with EtOH, prepared at various concentrations, and filtered through a 0.45 µm filter.

To investigate the antioxidant activity of each sample, equal amounts of the 0.5 mM DPPH solution and each antioxidant solution were mixed, and 500 µL of the mixture was immediately transferred to an ESR quartz flat cell (ES-LC12; JEOL Ltd., Tokyo, Japan). The ESR flat cell was placed in the cavity of the spectrometer, and ESR spectra were recorded over time. The ESR spectra were recorded on a JES-FA200 (JEOL Ltd., Japan) spectrometer operating at the X-band and 100 kHz field modulation. Care was taken to ensure that no saturation occurred and that the line shape was not distorted by excessive modulation amplitude. From a plot of the square root of the microwave power versus the signal peak height, a microwave power level of 4 mW was chosen. The ESR spectral intensity was determined by double integration. The magnetic field was set at 336.8 mT; field sweep, 7 mT; modulation amplitude, 1.0 G; time constant, 300 ms; sweep time, 15 min.

The hyperfine splitting constants were calculated by the splitting of MnO (ΔH = 8.69 mT). The radical scavenging activity was calculated by comparing the double-integrated values of the ESR spectra obtained from each sample and the control group, using Equation (2).

$$\text{Antioxidant activity } (\%) = 100 \times \left(1 - \frac{\text{double} - \text{integrated value of ESR spectrum in sample}}{\text{double} - \text{integrated value of ESR spectrum in control}}\right), \quad (2)$$

2.5. Cell Culture

Primary normal human dermal fibroblasts (NHDFs) were purchased from Zen-Bio, Inc. (Durham, NC, USA). NHDFs were grown in DMEM supplemented with 10% heat-inactivated fetal bovine serum (FBS), 100 U/mL penicillin, and 100 μg/mL streptomycin at 37 °C under 5% CO_2 in a humidified incubator. The NHDFs were passaged by trypsinization with EDTA aqueous solution and 0.25% trypsin-EDTA every three days, and the cells were used in the subsequent experiments. The NHDFs were passaged at least three times after initial culture, and all experiments were conducted using NHDFs obtained from fewer than 10 passages to prevent cellular senescence.

2.6. Cell Viability Assay

NHDF cell suspensions (2.0×10^4 cells/well) were seeded in 96-well plates and then incubated for 24 h at 37 °C under 5% CO_2 in a humidified incubator. The medium was replaced with 90 μL of fresh medium, and 10 μL of each antioxidant compound aqueous solution was added. The mixture was then incubated for 48 h at 37 °C under 5% CO_2 in a humidifier. The medium was then removed, the cells were quickly washed three times with pH 7.4 PBS, and 90 μL of fresh medium was added. 2-(4-Iodophenyl)-3-(4-nitrophenyl)-5-(2,4-disulfophenyl)-2H-tetrazolium sodium salt (WST-1, Dojindo Laboratory, Kumamoto, Japan) was dissolved in 20 mM pH 7.4 HEPES buffer to prepare a 5.5 mM WST-1 solution, and 1-methoxy-5-methylphenazinium methylsulfate (1-methoxy PMS, Dojindo Laboratory, Kumamoto, Japan) was dissolved in sterile water to prepare a 2 mM 1-methoxy PMS solution. Then, 5.5 mM WST-1 and 2 mM 1-methoxy PMS solutions were mixed at a ratio of 19 to 1 and then filtered through a 0.22 μm sterile membrane filter (Millex-GV Syringe Filter Unit, Millipore Corp., Bedford, MA, USA). WST-1 reagent solution (10 μL) was added to each well, and the plate was incubated for 2 h at 37 °C under 5% CO_2 in a humidified incubator. The absorbance of each well was measured at 450 nm. The percentage of cell viability was calculated using Equation (3).

$$\text{Cell viability } (\%) = \left[\frac{\left(\text{Abs.}_{\text{Experimental}} - \text{Abs.}_{\text{Negative control}}\right)}{\left(\text{Abs.}_{\text{Positive control}} - \text{Abs.}_{\text{Negative control}}\right)}\right] \times 100, \quad (3)$$

where $\text{Abs.}_{\text{Experimental}}$ is the absorbance of each sample, $\text{Abs.}_{\text{Negative control}}$ is the absorbance without cells, and $\text{Abs.}_{\text{Positive control}}$ is the absorbance of the confluent cells.

2.7. Quantification of Intracellular ROS in NHDF Exposed to UV-A with CLSM

An NHDF suspension (1.0×10^5 cell/mL) was seeded in a 35 mm cell culture dish and then incubated for 24 h at 37 °C under 5% CO_2 in a humidified incubator. After removing the medium, 2 mL of CPD diluted with DMEM (10~200 μg/mL as polyphenol concentration) was added to the cells and incubated for 2 h at 37 °C under a 5% CO_2 humidifier. The medium was replaced with fresh medium. The UV-A light (FL10BL, HotaluX Co., Ltd., Tokyo, Japan) was placed 100 mm above the cell culture dishes to provide irradiation for 15 min (8.6 mJ/cm^2), 30 min (17.1 mJ/cm^2), 45 min (25.7 mJ/cm^2), and 60 min (34.2 mJ/cm^2). To detect intracellular ROS, 2′,7′-dichlorodihydrofluorescein diacetate (DCFH-DA) purchased from Funakoshi Co., Ltd. (Tokyo, Japan) was used.

Non-fluorescent DCFH-DA is deacetylated by intracellular esterases to non-fluorescent DCFH, which is then quickly oxidized by intracellular ROS to form fluorescent 2′,7′-dichlorofluorescein (DCF). DCF has an excitation wavelength of 485 nm and an emission wavelength between 500 and 550 nm. The medium was removed after UV-A irradiation, and 2 mL of 60 μM DCFH-DA solution dissolved in 5 mL of DMSO and 95 mL of phenol red-free DMEM was added to the cells and then incubated for 1 h in the dark at 37 °C. The cells were washed three times with phenol red-free DMEM. Then, 2 mL of a 7.1 μg/mL Hoechst®33342 (DOJINDO, Kumamoto, Japan) aqueous solution dissolved in pH 7.4 PBS was added to the cells for nucleus staining and incubated for 10 min in the dark at 37 °C. After the solution was removed, the cells were quickly washed three times with pH 7.4 PBS. The solution was replaced with 2 mL of FluoroBrite DMEM (Gibco, Thermo Fisher Scientific Inc., Waltham, MA, USA) at 37 °C, and live-cell imaging was performed with a confocal laser scanning microscope LSM 900 (CLSM, Carl Zeiss, Jena, Germany). The fluorescence intensity of the image was quantified by Zeiss Zen 3.8 software.

2.8. ELISA for Quantification of MMP-1 Expression

MMP-1 produced by NHDFs exposed to UV-A was measured with a commercial ELISA kit (MMP-1 Human ELISA Kit, RayBiotech Inc., Norcross, GA, USA) according to the protocol. The resulting medium of NHDFs exposed to UV-A was incubated for 3 days and centrifuged (1500 rpm, 4 °C, 10 min). The isolated supernatant was prepared at an 8× dilution with buffer solution. All reagents and samples for the ELISA were brought to room temperature before use. The supernatant (100 μL) was added to a 96-well microplate and incubated for 2.5 h on a shaker at 500 rpm. The mixture was washed four times with 300 μL of wash solution. The biotinylated anti-MMP-1 detection antibody solution (100 μL) was added and incubated for 1 h on a shaker at room temperature. After each well was washed four times with PBS, 100 μL of streptavidin solution was added and incubated for 45 min on a shaker at 500 rpm. After additional washes with PBS, 100 μL of 3, 3′, 5, 5′-tetramethyl benzidine was added and incubated for 30 min on a shaker in the dark. After the addition of 50 μL of stop solution, the absorbance of each well at 450 nm was measured with a GloMax® Discover/Explorer System. The results obtained were analyzed using GainData® (arigo's ELISA Calculator, arigo Biolaboratories, Hsinchu, Taiwan), and MMP-1 concentrations were calculated.

2.9. Preparation of Three-Dimensional Collagen Gel Containing NHDFs

The three-dimensional collagen gel was constructed by first creating a base layer, then layering a cell suspension onto a collagen gel layer. The base layer was prepared to prevent NHDFs from adhering to the culture dish surface and forming a monolayer before collagen gelation. Briefly, 1.2 mL of five-times-concentrated DMEM, 2.2 mL of sterile water, and 0.6 mL of FBS were mixed in an ice bath, followed by the addition of 2.0 mL of 3 mg/mL acid-extracted collagen type I solution (Bovine skin, Lot. BSA 125B026, Nippi Co., Ltd., Tokyo, Japan) dissolved in 5 mM acetic acid aqueous solution and further mixing. Then, 1.0 mL of this mixture was dispensed into 35 mm Petri dishes and incubated for 2 h in a 5% CO_2 humidifier at 37 °C. Gelation was observed under a microscope. Secondly, 0.6 mL of five-times-concentrated DMEM, 0.1 mL of sterile water, 0.3 mL of FBS, and 3.0 mL of cell suspension (1.0×10^5 cells/mL) were mixed in an ice bath. Then, 2.0 mL of acid-extracted collagen solution was added and mixed. A total of 2.0 mL of the mixture was dispensed onto the base layer and incubated for 2 h in a 5% CO_2 humidifier at 37 °C to form gels. After gelation, 2.0 mL of medium was added, and thereafter, the medium was replaced every 2 days.

2.10. Evaluation of Elastic Properties of Collagen Gels Using Dynamic Mechanical Analysis (DMA)

The mechanical properties of collagen gels were evaluated using compression testing with dynamic mechanical analysis (DMA Q800, TA Instruments, New Castle, DE, USA). Collagen gels with a diameter of 35 mm and a thickness of 1–2 mm were used for the test. The gel was placed between compression plates, and each measurement was performed at 37 °C. An initial load of 0.01 N was applied, and compression was then performed at a constant rate (0.5 N/min) to obtain the stress–strain curve. The Young's modulus (E) of each gel was calculated from the slope of the linear region of the obtained stress–strain curve, using Equation (4).

$$\text{Young's modulus (Pa)} = \Delta \text{ stress (Pa)}/\Delta \text{ strain}, \quad (4)$$

2.11. Effect of CPD Pretreatment on Weight Loss of UV-A-Exposed Collagen Gels

Prior to UV-A irradiation for 60 min, each collagen gel embedded with NHDFs was pretreated with predetermined concentrations of CPD (0, 20, 100, and 200 μg/mL) and then incubated for 7 days at 37 °C in a 5% CO_2 humidifier. Subsequently, each gel was immersed in ethanol, and the mass of the remaining gel after removing the ethanol solution was measured. Each relative value was calculated using the mass of the blank gel without UV-A irradiation.

3. Results

3.1. HPLC and SEC Analysis of CPD and Its Antioxidant Effect

The filtrate and the residue of CPD extracted with fermentation medium were analyzed by high-performance liquid chromatography (HPLC). Figure S1 shows that no difference was observed between the HPLC results from the filtrate and residue, suggesting that the broad peak of the main five components originated from polymers composed of CPD. It can also be seen in Figure S2 that a peak originating from the polymer was observed in the SEC measurements, and the number-average molecular weight (M_n) of the polymer, such as polyphenols, contained in the CPD was 9800 g mol^{-1} (M_w/M_n = 1.58). The polyphenol concentrations before and after fermentation using the fermentation medium were 0.9 mg/mL and 1.1 mg/mL, respectively. These results suggest that CPD is mainly composed of polyphenolic compounds derived from Chaga, and the molecular weight of the main polymer was 9800 g mol^{-1}.

To suppress intracellular oxidative stress, it is important to gain fundamental insights into the antioxidant properties of CPD. 1,1-Diphenyl-2-picryl-hydrazyl (DPPH) is a stable free radical at room temperature in air and can be converted into its molecular form by abstracting a hydrogen atom from antioxidant compounds. Therefore, the antioxidant activity can be estimated from the percentage reduction in spectral intensity measured by ESR spectroscopy of DPPH. Since Chaga mushroom contains high-molecular-weight lignin and low-molecular-weight caffeic acid as two of its main components [18–20], the radical scavenging effects of these compounds were compared with those of CPD. As shown in Figure 2a, DPPH as a blank exhibited a characteristic quintet spectrum due to the coupling of the nitrogen-centered radical (g = 2.0036) with two nitrogen atoms, and the difference between the maximum and minimum peak intensities was approximately 12,000. Meanwhile, the ESR spectral intensities of DPPH were significantly decreased without any changes in the spectral form when each antioxidant compound was added to DPPH at different concentrations, and the peak intensities were reduced to below 3000 in all cases. Caffeic acid and CPD scavenged most of the DPPH radicals at concentrations around 50 μg/mL. It can be seen in Figure 2b that CPD exhibited antioxidant effects at the lowest concentration, followed by caffeic acid and then lignin. The IC_{80} values indicating

the concentration at which the majority of DPPH radicals were scavenged were 33, 50, and 200 µg/mL for CPD, caffeic acid, and lignin, respectively. These results suggest that CPD is useful as a free radical scavenger in solution.

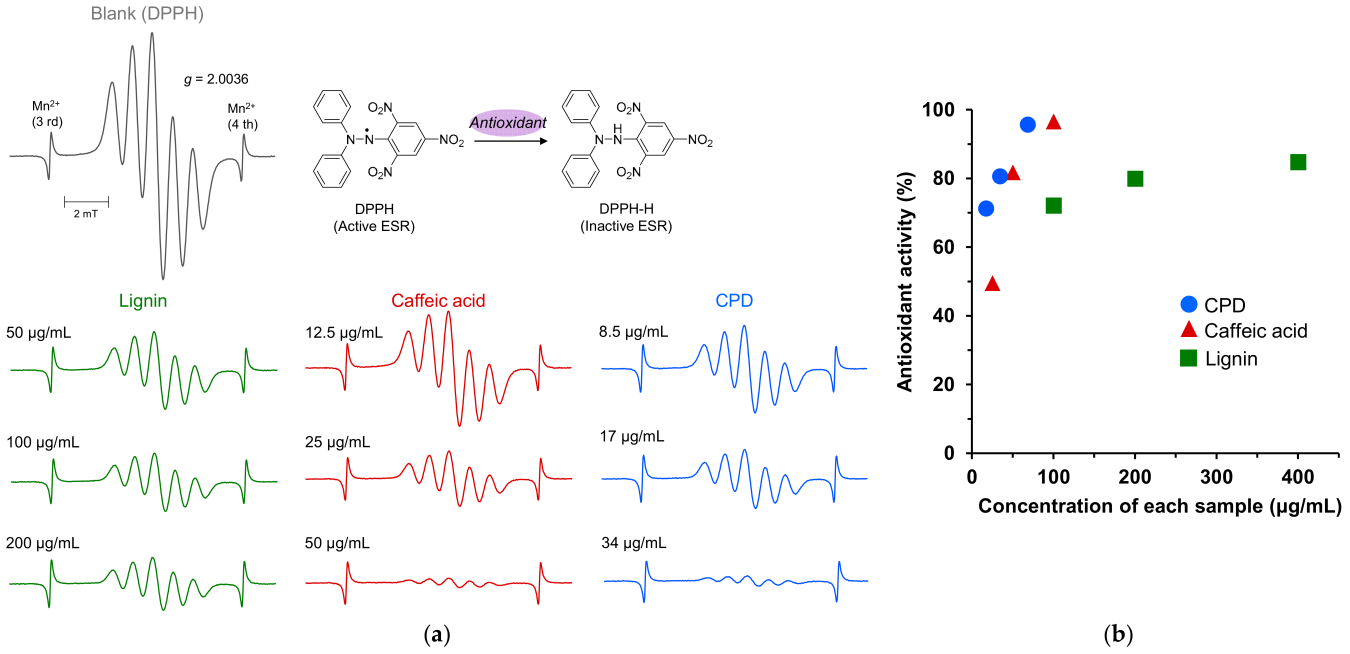


Figure 2. (**a**) ESR spectra of DPPH (blank) and samples treated with lignin, caffeic acid, and CPD. (**b**) Antioxidant activity determined by the double integration of ESR spectra using Equation (2).

3.2. Intracellular ROS Generated in NHDFs Exposed to UV-A and Its Suppression by CPD

The ROS generated in cells vary greatly depending on the location of expression. ROS generated around the cell membrane may cause lipid peroxidation and inhibit the mitochondrial electron transport system, and cell death can finally be induced [29–31]. Therefore, the observation of CLSM using imaging agents that emit fluorescence in response to ROS generated in cells reveals the localization and amount of ROS through brightness analysis. Hong et al. have reported that polyphenols can reliably penetrate cell membranes within 2 h by pre-incubating the cells [32]. Our previous study revealed that the cell viability of NHDFs was maintained up to 60 min (34.2 mJ/cm^2) of UV-A exposure, whereas an exposure time of more than 90 min (51.3 mJ/cm^2) markedly reduced their viability. Therefore, the UV-A irradiation time for NHDFs was limited to 60 min in this study, as shown in Figure S3 [22]. DCFH-DA, which can penetrate the cell membrane, was used as an intracellular ROS detection agent. DCFH-DA is capable of crossing the plasma membrane to enter the interior of cells, where cellular esterases hydrolyze its acetyl moieties to produce DCFH [33–35]. The generated DCFH changes to fluorescein DCF (λ_{ex}.: 485 nm, λ_{em}.: 500~550 nm) based on the oxidation by ROS, and the amount of intracellular ROS production can be evaluated by measuring the fluorescence intensity of DCF. In addition, nuclear staining of NHDFs was performed using Hoechst®33342 (Dojindo Laboratories, Kumamoto, Japan), which can stain the nucleus of living cells, and live-cell imaging was carried out by CLSM at room temperature. Figure 3a shows the DCF-derived fluorescence generated in NHDFs exposed to UV-A without CPD pretreatment. The overlay between the phase-contrast image representing cell morphology and the green fluorescent image of DCF reveals the expression of intracellular ROS, indicating that ROS remained intracellular.

The expression of the ROS generated in NHDFs exposed to UV-A was widespread throughout the cytosol and was also detected in the nucleus. Since the fluorescence intensity of DCF increased with the extension of the UV-A irradiation time, ROS continued

to be produced without saturation until 60 min of UV-A irradiation. The addition of 10% (v/v) pH 7.4 PBS to the medium did not result in any difference in ROS production from NHDF cells. Figure 3b also shows confocal images of the cells exposed to UV-A after pretreatment with CPD. The live cell was confirmed by the phase-contrast microscopy image and the blue fluorescent image of Hoechst®33342, and DCF-derived fluorescence was significantly suppressed even after 60 min of UV-A irradiation. The CLSM images of DCF-derived green fluorescence were quantitatively analyzed as the median fluorescence intensity of 5 μm width × 5 μm height. It can also be seen in Figure 3c that the mean fluorescence intensity (73,600) of DCF in NHDFs not treated with CPD after 60 min of UV-A irradiation was 4.3 times higher than that of the CPD-pretreated group (mean fluorescence intensity: 17,100). The ANOVA analysis of Figure 3c revealed significant differences ($p = 3.76 \times 10^{-18}$; F = 3.95) between the two groups with or without CPD pretreatment and the UV-A irradiation time. Caffeic acid and lignin, which exhibit antioxidant activity, were similarly evaluated as positive controls for comparison with CPD. As shown in Figure 3d, the WST-1 assay revealed that all three compounds at concentrations of 200 μg/mL showed a slight cytotoxicity of 25% or less toward NHDFs after 48 h of incubation. Therefore, it was inferred that cytotoxicity does not occur during the 4 h pretreatment with these antioxidants. After pretreating NHDFs with caffeic acid or lignin at a final concentration of 200 μg/mL, ROS generation in the NHDFs following 60 min of UV-A irradiation was evaluated with CLSM based on DCF-derived fluorescence, as shown in Figure 3e. It can also be seen in Figure 3f that CPD exhibited the lowest DCF-derived fluorescence intensity, followed by caffeic acid and then lignin. Each polyphenol concentration was measured using the Folin–Ciocalteu method and converted to gallic acid equivalents, as shown in Figure S4. Table 1 shows that the polyphenol concentrations of CPD, caffeic acid, and lignin were 127.4, 114, and 91 μg/mL, respectively, at a solute concentration of 200 μg/mL. These results suggest that antioxidant activity against NHDFs exposed to UV-A is due to the polyphenol concentration.

To clarify the required dosage of CPD for antioxidant activity, CPD prepared at a polyphenol concentration of 10~100 μg/mL was administered to NHDFs, intracellular ROS were observed using CLSM, and the fluorescence intensity was quantitatively analyzed. Figures 4a and S5 show that the DCF-derived fluorescence decreased with increasing CPD concentration. A significant difference in DCF-derived fluorescence was observed between 20 μg/mL of CPD and the control, as shown in Figure 4b. It has been reported that an extract derived from *Dipterocarpus tuberculatus*, containing low-molecular-weight antioxidant phenolic compounds (100–400 μg/mL), could inhibit cell death in NHDF exposed to UV-A in a concentration-dependent manner and that the generation of reactive nitrogen species such as nitric oxide was almost completely suppressed at 400 μg/mL [36]. The ROS amount based on the mean fluorescence intensity (1700) of DCF in 100 μg/mL of CPD was suppressed to less than 5% compared to the control (mean fluorescence intensity: 73,600). The ANOVA analysis of Figure 4b revealed that significant differences ($p = 5.98 \times 10^{-7}$, F = 2.38) in fluorescence intensity from intracellular DCF were observed with or without CPD pretreatment at each concentration. It was thus demonstrated that CPD possessed antioxidant activity capable of quenching most of the ROS generated from NHDF cells exposed to UV-A, even at 100 μg/mL. These findings suggest that the expression of the ROS generated in NHDF exposed to UV-A was widespread throughout the cells and may induce skin problems. CPD may thus protect NHDFs from ROS generated by UV-A irradiation.

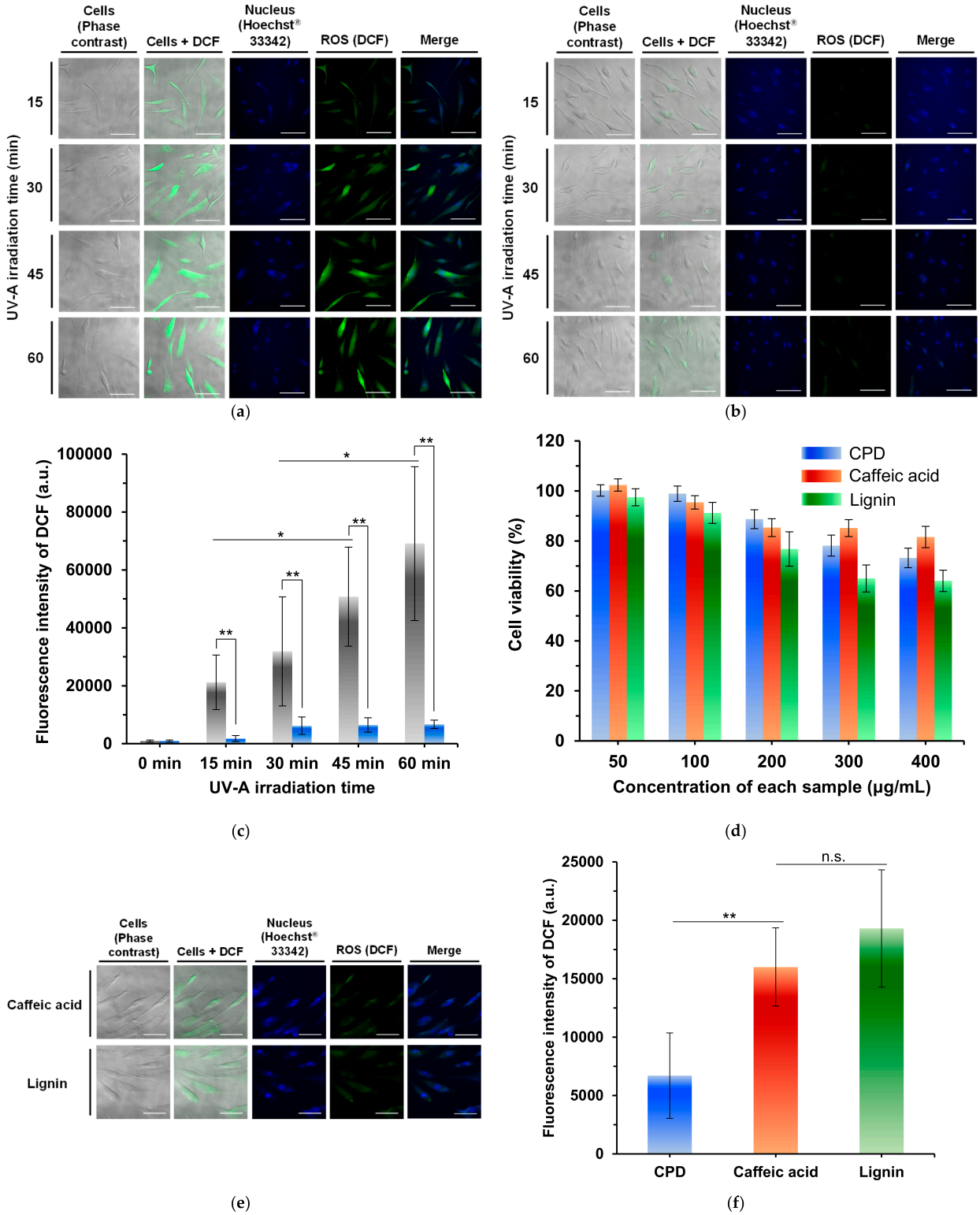


Figure 3. Progressive changes in the intracellular distribution of ROS in NHDFs exposed to UV-A for 60 min without pretreatment with CPD (**a**), with pretreatment with CPD (**b**), and brightness analysis of intracellular ROS (**c**). Cell viability of NHDFs treated with each concentration of CPD, caffeic acid, and lignin (**d**). Confocal laser scan images of NHDFs exposed to UV-A for 60 min after pretreatment with 200 μg/mL of caffeic acid or lignin (**e**), and brightness analysis of intracellular ROS (**f**). The nucleus was stained with Hoechst 33342® (blue fluorescence). CPD was prepared at a polyphenol concentration of 200 μg/mL. Scale bar = 100 μm. Statistical analysis was performed using two-way ANOVA with repeated measures, and the statistical significance was measured between the two groups using Welch's *t*-test for unequal variances. * $p < 0.05$; ** $p < 0.0001$; n.s.: not significant.

Table 1. Polyphenol concentration of each antioxidant determined by the Folin–Ciocalteu method.

Antioxidants	Solute Concentration (μg/mL)	Absorbance	Polyphenol Concentration Expressed as Gallic Acid (μg/mL)
Lignin	200	0.1966	91.0
Caffeic acid	200	0.2474	114.0
CPD	200	0.2770	127.4

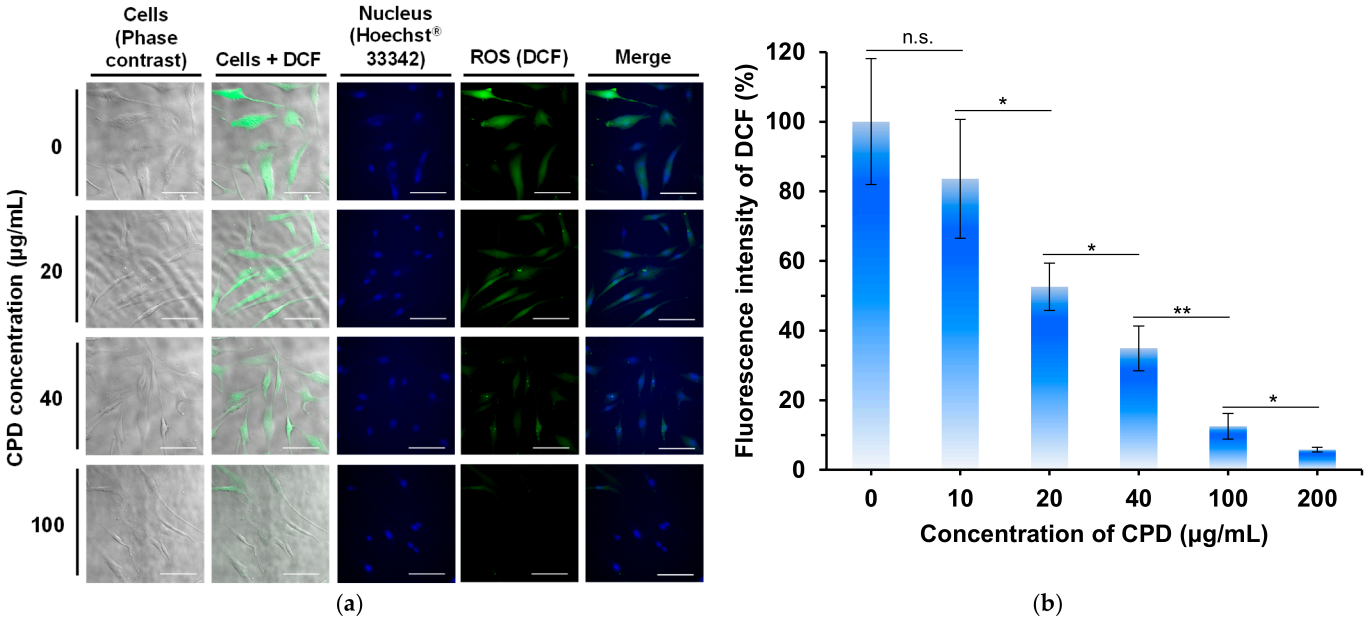


Figure 4. (**a**) CLSM images of NHDFs exposed to UV-A for 60 min after pretreatment with each concentration of CPD (scale bar = 100 μm). (**b**) Fluorescence intensity of DCF determined by brightness analysis of CLSM images. Data are shown as the mean ± SD (n = 10). Statistical analysis was performed using one-way ANOVA, and statistical significance was measured between two groups using Welch's *t*-test for unequal variances. * $p < 0.05$; ** $p < 0.01$; n.s.: not significant.

3.3. The Expression Levels of MMP-1 Produced from NHDFs Exposed to UV-A and the Inhibitory Effects of CPD

The expression of ROS generated in NHDFs may lead to the inhibition of DNA repair and overexpression of mRNA by stimulating the nucleus. Since the overexpression of mRNA for pre-MMP-1 enhances the expression of MMP-1, the degradation of collagen in the skin may be induced [37]. Therefore, the inhibition of ROS suppresses the degradation of collagen, owing to a reduction in MMP-1 expression. The quenching of ROS by CPD prevents the dermal fragility caused by collagen degradation. The supernatant of the culture medium of NHDFs exposed to UV-A irradiation was investigated with ELISA for the measurement of MMP-1 expression, as shown in the calibration curve in Figure S6. Figures 5a and S7 show the expression level of MMP-1 for a predetermined UV-A irradiation time. The expression of MMP-1 in NHDFs without pretreatment with CPD increased with UV-A irradiation time, and 60 min of UV-A irradiation produced 26.7 ng/mL of MMP-1. The ANOVA analysis of Figure 5a revealed significant differences ($p = 8.7 \times 10^{-15}$; F = 4.35) between the two groups regarding the presence or absence of CPD pretreatment and UV-A irradiation time. As shown in Figure 5b, pretreatment with 200 μg/mL of CPD successfully suppressed MMP-1 production at approximately 8.8 ng/mL in experimental conditions similar to those described above. It was thus revealed that MMP-1 expression based on the antioxidant effect of CPD was suppressed by 33% compared to that without CPD. Furthermore, a statistically significant difference ($p < 0.05$) between the presence and absence of CPD pretreatment was observed after 30 min of UV-A irradiation, and

prolonged irradiation made the significant difference ($p < 0.01$) more precise. These findings suggest that CPD may contribute to the prevention of wrinkle formation by inhibiting the expression of MMP-1 in UV-A-irradiated skin.

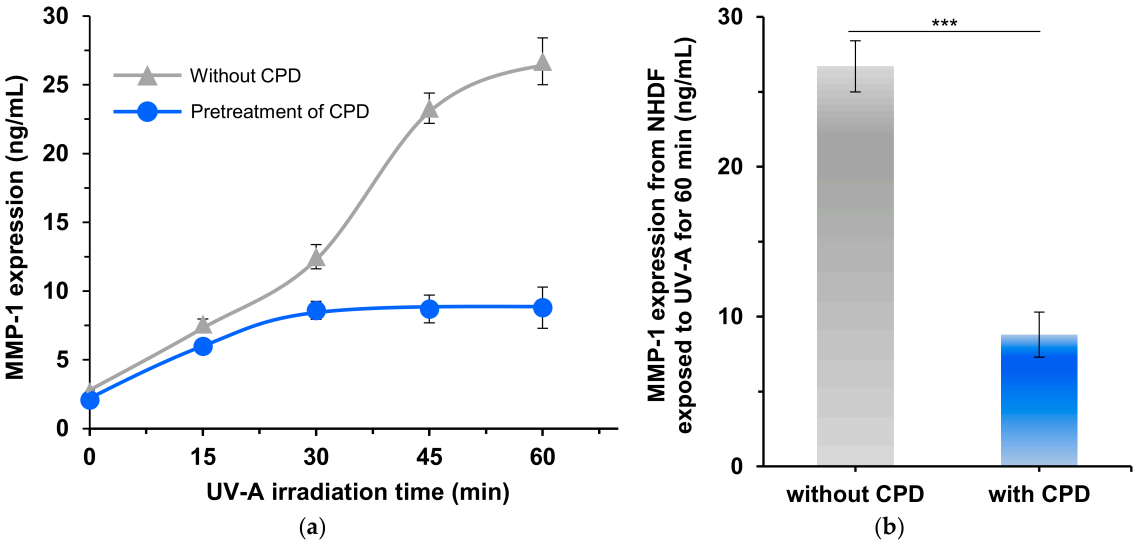


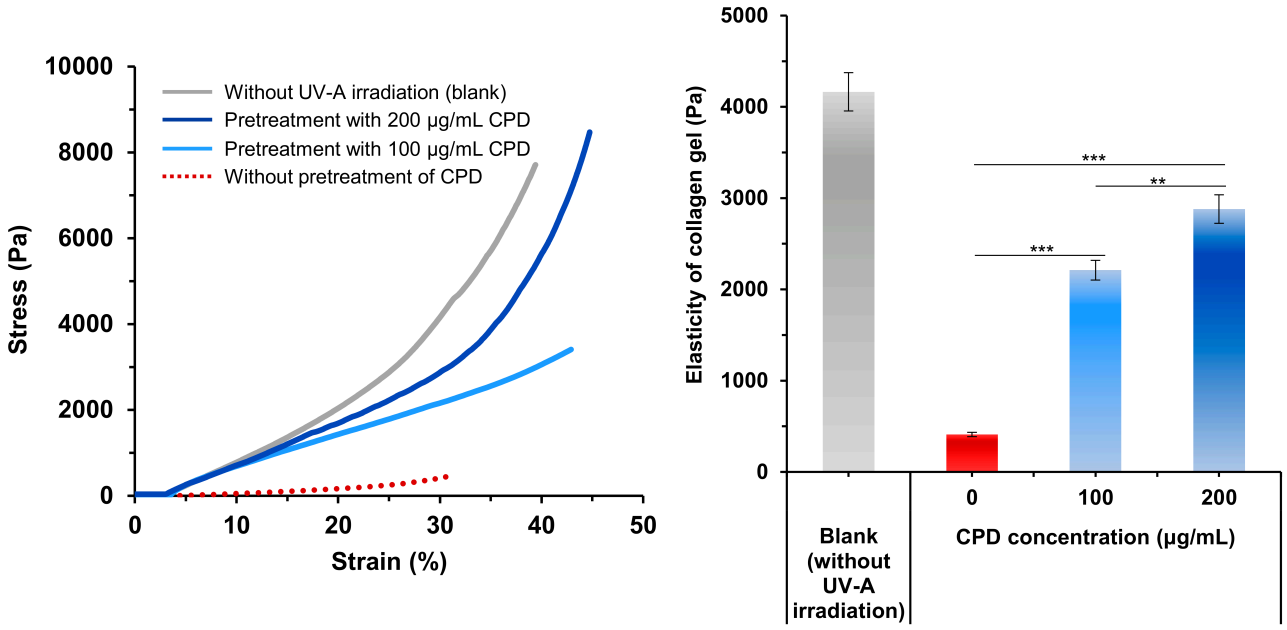
Figure 5. (**a**) Progressive changes in MMP-1 production from NHDFs with UV-A irradiation time. (**b**) Suppression effect of CPD on MMP-1 production in NHDFs exposed to UV-A for 60 min. Data are shown as the mean ± SD (n = 3). Statistical analysis was performed using two-way ANOVA with repeated measures, and statistical significance was measured between two groups using Welch's *t*-test for unequal variances. *** $p < 0.001$.

3.4. Evaluation of Elastic Properties in Skin-Mimetic Models

In the previous subsection, it was demonstrated that CPD significantly suppressed MMP-1 production from NHDFs exposed to UV-A. Although the suppression of MMP-1 expression is advantageous for skin tissues, the inhibitory effect of CPD on collagen degradation was not directly demonstrated. Therefore, we aimed to investigate the inhibitory effect of CPD on collagen degradation using an evaluation system closer to skin tissue. Since approximately 70% of human dermis consists of collagen, a collagen gel containing NHDFs is a useful tool for a three-dimensional model mimicking the dermis. We verified whether pretreatment with CPD during UV-A exposure of collagen gel containing NHDFs suppresses collagen degradation, thereby maintaining the elasticity of the collagen gel. The elastic behavior of this skin-mimetic model was analyzed to verify the inhibitory effect of collagen degradation by CPD based on its three-dimensional physical properties. The elasticity of collagen gel strongly depends on the maintenance of its fiber structure and crosslink density; thus, it is known that the mechanical strength of the gel decreases as degradation progresses [38–40]. Therefore, Young's modulus was calculated from the linear region of the stress–strain curve obtained using dynamic mechanical analysis (DMA) and used as an indicator of collagen gel elasticity. The collagen gel prepared in a 35 mm Petri dish adhered stably to the DMA apparatus table without falling off. Since DMA measurements of collagen gels and films exhibited linear behavior when the strain rate was between 0.0001 and 0.1 N/s, the measurements in this study were performed at a strain rate of 0.008 N/s [41–43].

The prepared collagen gel was treated with CPD at concentrations ranging from 0 to 200 μg/mL, irradiated with UV-A for 60 min, and then incubated for 7 days. The incubated gels were compressed at a constant rate (0.008 N/s) via DMA measurement to obtain stress–strain curves. As shown in Figure 6a and the slopes in Figures S8–S11, the UV-A-irradiated group without CPD pretreatment exhibited a 91% reduction in Young's modulus

determined by Equation (4), compared to the non-UV-A-irradiated group, indicating a significant decrease in elasticity. The UV-A-irradiated gel without pretreatment with CPD reached the detection limit early during compression, even before DMA measurement, due to its thinner gel thickness compared to other gels, suggesting structural weakening associated with collagen degradation. As is evident from Figure 6b, the reduction in Young's modulus was clearly suppressed in CPD-pretreated gels in accordance with the CPD concentration. In gels treated with CPD at 200 µg/mL, the decrease in Young's modulus was only 35% compared to the UV-A-untreated blank, as shown in Figures S8 and S9. The ANOVA analysis of Figure 6b revealed significant differences in the stress values (p = 7.0 × 10^{-9}; F = 4.07) of collagen gels with or without pretreatment with CPD at each concentration. Therefore, UV-A irradiation induced MMP-1 expression from NHDFs embedded in collagen, which led to the degradation of collagen fibers constituting the gel and a significant decrease in gel elasticity. However, pretreatment with CPD suppressed this elasticity loss, demonstrating that the structural stability of the skin-mimicking gel is maintained.



(**a**) (**b**)

Figure 6. (**a**) Progressive changes in the typical stress–strain relationship of each collagen gel. (**b**) Comparison of the elasticity of each collagen gel. Data are shown as the mean ± SD (n = 3). Statistical analysis was performed using one-way ANOVA, and statistical significance was measured between two groups using Welch's *t*-test for unequal variances. ** $p < 0.01$, *** $p < 0.001$.

It is well-known that collagen degraded by MMP-1 becomes soluble in EtOH [44–46]. Then, the UV-A-irradiated gel, after pretreatment with CPD, was immersed in EtOH, and the weight of the gel after removing the ethanol was measured. As shown in Figures 7 and S12, the weight loss of the UV-A-irradiated gel without CPD pretreatment was approximately 30% compared to the blank gel without UV-A irradiation. However, pretreatment with CPD suppressed the weight loss of UV-A-irradiated gel in a concentration-dependent manner. The collagen gel pretreated with 200 µg/mL CPD retained approximately 97% of its weight after UV-A irradiation. The ANOVA analysis of Figure 7 revealed significant differences in the weights (p = 1.14 × 10^{-4}; F = 3.48) of collagen gels with or without pretreatment with CPD at each concentration. These results indicate that CPD significantly suppresses collagen degradation induced by UV-A irradiation.

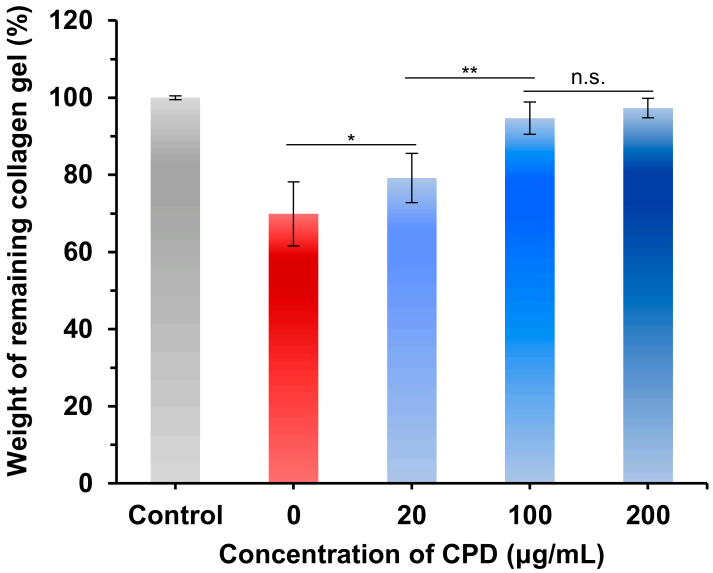


Figure 7. Weight loss of collagen gel exposed to UV-A and the suppressive effect of CPD. Data are shown as the mean ± SD (n = 3). Statistical analysis was performed using one-way ANOVA, and statistical significance was measured between two groups using Welch's *t*-test for unequal variances. * $p < 0.05$; ** $p < 0.01$; n.s.: not significant.

4. Discussion

As is evident from Figure 3, ROS expression was observed not only in the cytoplasm but also within the nucleus in NHDFs exposed to UV-A for 60 min. Oxidative stress caused by ROS leads to cell death and reduced skin tissue elasticity. Indeed, both in prior studies [22] and this research, it was revealed that NHDFs exposed to UV-A for over 90 min exhibited a dramatic decrease in cell viability and collagen degradation, potentially induced by MMP-1 expression. Pretreatment of NHDFs with CPD could, however, reduce UV-A-induced cytotoxicity and MMP-1 expression by suppressing ROS production. Figure 5 shows that up to 15 min of UV-A exposure, there was no difference in MMP-1 expression from NHDFs with or without CPD pretreatment. However, a significant difference in MMP-1 expression emerged over 30 min of UV-A exposure. As clearly shown in Figure 3, short-term UV-A exposure suppressed intracellular ROS generation. However, UV-A exposure exceeding 30 min increased ROS production and the associated MMP-1 expression in NHDFs, and CPD pretreatment was advantageous for suppressing these effects. Furthermore, elasticity evaluation using a three-dimensional collagen gel revealed that over 90% of elasticity was lost after 60 min of UV-A irradiation, and approximately 35% of collagen was degraded, as determined by the loss of gel mass. This UV-induced photoaging was significantly mitigated by CPD administration, since gel elasticity and mass loss were reduced to 35% and only 3%, respectively. These results suggest that CPD may contribute to protective effects on collagen and NHDFs.

5. Conclusions

Elucidating the antioxidant effect of Chaga polyphenol in quenching ROS generated in cells is crucial in preventing skin aging and inflammation. In this study, ROS expression from normal human dermal fibroblasts (NHDFs) exposed to UV-A with or without pretreatment with Chaga polyphenol decoction (CPD) was examined using live-cell imaging. In an investigation of radical scavenging activity using 1,1-Diphenyl-2-picryl-hydrazyl (DPPH), the ESR spectral intensities of DPPH with added CPD decreased more than those of lignin and caffeic acid. Cells pretreated with CPD at concentrations of 20 μg/mL or higher showed significant suppression of ROS production compared to the untreated con-

trol, and ROS production from NHDFs pretreated with 100 μg/mL CPD decreased to less than 5%. Furthermore, UV-A-irradiated NHDFs exhibited uniform ROS production within the cells, and CPD comprehensively reduced the generated ROS. Since ROS generated within cells also induce the overexpression of the MMP-1 precursor and its mRNA, MMP-1 produced by the activation of the MMP-1 precursor may decompose the collagen in the dermis, which can lead to wrinkles due to reduced skin elasticity. The expression level of MMP-1 was thus investigated using ELISA. In cells pretreated with CPD, the MMP-1 expression level was reduced to less than one-quarter of that in untreated cells. Furthermore, an NHDF-embedded three-dimensional collagen gel exposed to UV-A maintained an elasticity more than seven times higher than that of the blank gel due to pretreatment with CPD. These results verify the effective anti-ROS activity of CPD.

Supplementary Materials: The following supporting information can be downloaded at https://www.mdpi.com/article/10.3390/cosmetics13040167/s1, Figure S1: HPLC chromatogram of the filtrate and residue of CPD; Figure S2: SEC chromatogram of CPD; Figure S3: Cell viability of NHDFs exposed to UV-A at each irradiation time; Figure S4: Calibration curve of gallic acid (a), lignin (b), caffeic acid (c), and CPD (d) in Folin-Ciocalteu method; Figure S5: CLSM images of NHDFs exposed to UV-A for 60 min after pretreatment with CPD at 10 or 200 μg/mL. (Scale bar = 100 μm); Figure S6: MMP-1 calibration curve for ELISA assay; Figure S7: ELISA assay results of MMP-1 produced by NHDFs exposed to each UV-A irradiation time; Figure S8: Stress-strain curves of three-dimensional collagen gel as blank; Figure S9: Stress-strain curves of three-dimensional collagen gel pretreated with 200 μg/mL CPD after 60 min of UV-A irradiation; Figure S10: Stress-strain curves of three-dimensional collagen gel pretreated with 100 μg/mL CPD after 60 min of UV-A irradiation; Figure S11: Stress-strain curves of three-dimensional collagen gel without pretreatment of CPD after 60 min of UV-A irradiation; Figure S12: Stress-strain curves of three-dimensional collagen gel without pretreatment of CPD after 60 min of UV-A irradiation.

Author Contributions: Conceptualization, N.D. and M.K.; methodology, N.D. and S.E.; software, N.D.; validation, N.D. and Y.Y.; formal analysis, N.D., S.E., K.M., A.K., and Y.Y.; investigation, N.D., K.M., A.K., and S.E.; resources, N.D. and K.A.; data curation, N.D.; writing—original draft preparation, N.D. and S.E.; writing—review and editing, N.D. and S.-i.K.; visualization, N.D.; supervision, N.D. and M.K.; project administration, N.D.; funding acquisition, N.D. and K.A. Author M.K. passed away prior to the publication of this manuscript. All authors have read and agreed to the published version of the manuscript.

Funding: This work was financially supported by JSPS KAKENHI (grant number 25K09926), the Amano Institute of Technology, the Takeda Science Foundation, the Izumi Science and Technology Foundation, and the Uehara Memorial Foundation.

Institutional Review Board Statement: Not applicable.

Informed Consent Statement: Not applicable.

Data Availability Statement: The original contributions presented in this study are included in the article. Further inquiries can be directed to the corresponding author.

Conflicts of Interest: Kazuichi Araki is employed by Be·GLAD ichiyo Co., Ltd. The sample of Chaga Polyphenol Docoction was received from Be·GLAD ichiyo Co., Ltd. All authors declare that the research was conducted in the absence of any commercial or financial relationships that could be construed as a potential conflict of interest. The funder had no role in the design of the present study; in the analysis or interpretation of data; in the writing of the manuscript; or in the decision to publish the results.

Abbreviations

The following abbreviations are used in this manuscript:

CLSM	Confocal Laser Scanning Microscopy
CPD	Chaga Polyphenol Decoction
DCFH	2, 7-Dichlorodihydrofluoresceine
DCFH-DA	2, 7-Dichlorodihydrofluoresceine Diacetate
DMSO	Dimethyl Sulfoxide
DMA	Dynamic Mechanical Analysis
DMEM	Dulbecco's Modified Eagle Medium
DPPH	1,1-Diphenyl-2-picryl-hydrazyl
EDTA	Ethylenediaminetetraacetic Acid
ELISA	Enzyme-Linked Immunosorbent Assay
Ex	Excitation
Em	Emission
FBS	Fetal Bovine Serum
MMP-1	Matrix Metalloproteinase-1
NHDFs	Normal Human Dermal Fibroblasts
PBS	Phosphate-Buffered Saline
ROS	Reactive Oxygen Species
UV	Ultraviolet

References

1. Gardeazabal, L.; Izeta, A. Elastin and collagen fibres in cutaneous wound healing. *Exp. Dermatol.* **2024**, *33*, e15052. [CrossRef] [PubMed]
2. Pu, S.-Y.; Huang, Y.-L.; Pu, C.-M.; Kang, Y.-N.; Hoang, K.D.; Chen, K.-H.; Chen, C. Effects of Oral Collagen for Skin Anti-Aging: A Systematic Review and Meta-Analysis. *Nutrients* **2023**, *15*, 2080. [CrossRef] [PubMed]
3. Bravo, B.; Correia, P.; Gonçalves, J.E., Jr.; Sant'Anna, B.; Kerob, D. Benefits of topical hyaluronic acid for skin quality and signs of skin aging: From literature review to clinical evidence. *Dermatol. Ther.* **2022**, *35*, e15903. [CrossRef] [PubMed]
4. Juncan, A.M.; Moisă, D.G.; Santini, A.; Morgovan, C.; Rus, L.-L.; Vonica-Țincu, A.L.; Loghin, F. Advantages of Hyaluronic Acid and Its Combination with Other Bioactive Ingredients in Cosmeceuticals. *Molecules* **2021**, *26*, 4429. [CrossRef] [PubMed]
5. Ansary, T.M.; Hossain, M.R.; Kamiya, K.; Komine, M.; Ohtsuki, M. Inflammatory Molecules Associated with Ultraviolet Radiation-Mediated Skin Aging. *Int. J. Mol. Sci.* **2021**, *22*, 3974. [CrossRef] [PubMed]
6. Salminen, A.; Kaarniranta, K.; Kauppinen, A. Photoaging: UV radiation-induced inflammation and immunosuppression accelerate the aging process in the skin. *Inflamm. Res.* **2022**, *71*, 817–831. [CrossRef] [PubMed]
7. Liao, W.; Wang, Y.; Wang, Y.; Liao, J.; Chen, N.; Jia, C.; Zeng, L. Interplay of Skin Aging: Mitochondrial Stress and Ultraviolet Exposure. *Photodermatol. Photoimmunol. Photomed.* **2026**, *42*, e70089. [CrossRef] [PubMed]
8. Loo, Y.C.; Hu, H.-C.; Yu, S.-Y.; Tsai, Y.-H.; Korinek, M.; Wu, Y.-C.; Chang, F.-R.; Chen, Y.-J. Development on potential skin anti-aging agents of *Cosmos caudatus* Kunth via inhibition of collagenase, MMP-1 and MMP-3 activities. *Phytomedicine* **2023**, *110*, 154643. [CrossRef] [PubMed]
9. Feng, C.; Chen, X.; Yin, X.; Jiang, Y.; Zhao, C. Matrix Metalloproteinases on Skin Photoaging. *J. Cosmet. Dermatol.* **2024**, *23*, 3847–3862. [CrossRef] [PubMed]
10. Nagajyothi, P.C.; Sreekanth, T.V.M.; Lee, J.; Lee, K.D. Mycosynthesis: Antibacterial, antioxidant and antiproliferative activities of silver nanoparticles synthesized from *Inonotus obliquus* (Chaga mushroom) extract. *J. Photochem. Photobiol. B Biol.* **2014**, *130*, 299–304. [CrossRef]
11. Szychowski, K.A.; Skora, B.; Pomianek, T.; Gminski, J. *Inonotus obliquus*—From folk medicine to clinical use. *J. Tradit. Complement. Med.* **2021**, *11*, 293–302. [PubMed]
12. Nguyet, T.M.N.; Lomunova, M.; Le, B.V.; Lee, J.S.; Park, S.K.; Kang, J.S.; Kim, Y.H.; Hwang, I. The mast cell stabilizing activity of Chaga mushroom critical for its therapeutic effect on food allergy is derived from inotodiol. *Int. Immunopharmacol.* **2018**, *54*, 286–295. [CrossRef] [PubMed]
13. Liu, Z.; Yu, D.; Li, L.; Liu, X.; Zhang, H.; Sun, W.; Lin, C.-C.; Chen, J.; Chen, Z.; Wang, W.; et al. Three-phase partitioning for the extraction and purification of polysaccharides from the immunomodulatory medicinal mushroom *Inonotus obliquus*. *Molecules* **2019**, *24*, 403. [CrossRef] [PubMed]

14. Shibnev, V.A.; Mishin, D.V.; Garaev, T.M.; Finogenova, N.P.; Botikov, A.G.; Deryabin, P.G. Antiviral activity of *Inonotus obliquus* fungus extract towards infection caused by hepatitis C virus in cell cultures. *Bull. Exp. Biol. Med.* **2011**, *151*, 612–614. [CrossRef] [PubMed]
15. Zhang, C.-J.; Guo, J.-Y.; Cheng, H.; Li, L.; Liu, Y.; Shi, Y.; Xu, J.; Yu, H.-T. Spatial structure and anti-fatigue of polysaccharide from *Inonotus obliquus*. *Int. J. Biol. Macromol.* **2020**, *151*, 855–860. [CrossRef] [PubMed]
16. Yildiz, O.; Can, Z.; Laghari, A.Q.; Sahin, H.; Malkoc, M. Wild edible mushrooms as a natural source of phenolics and antioxidants. *J. Food Biochem.* **2015**, *39*, 148–154. [CrossRef]
17. Hu, Y.; Shi, S.; Lu, L.; Teng, C.; Yu, S.; Wang, X.; Yu, M.; Liang, J.; Qu, J. Effects of selenizing modification on characteristics and antioxidant activities of *Inonotus obliquus* polysaccharide. *Macromol. Res.* **2017**, *25*, 222–230. [CrossRef]
18. Hwang, A.Y.; Yang, S.C.; Kim, J.; Lim, T.; Cho, H.; Hwang, K.T. Effects of non-traditional extraction methods on extracting bioactive compounds from chaga mushroom (*Inonotus obliquus*) compared with hot water extraction. *LWT* **2019**, *110*, 80–84. [CrossRef]
19. Yong, T.; Chen, S.; Liang, D.; Zuo, D.; Diao, X.; Deng, C.; Wu, Y.; Hu, H.; Xie, Y.; Chen, D. Actions of *Inonotus obliquus* against Hyperuricemia through XOD and Bioactives Screened by molecular modeling. *Int. J. Mol. Sci.* **2018**, *19*, 3222. [CrossRef] [PubMed]
20. Lee, Y.; Shin, M.H.; Kim, M.-K.; Park, C.-H.; Shin, H.S.; Lee, D.H.; Chung, J.H. Ultraviolet irradiation-induced inhibition of histone deacetylase 4 increases the expression of matrix metalloproteinase-1 but decreases that of type I procollagen *via* activating JNK in human dermal fibroblasts. *J. Dermatol. Sci.* **2021**, *101*, 107–114. [CrossRef] [PubMed]
21. Podkawa, A.; Kryczyk-Poprawa, A.; Opoka, W.; Muszynska, B. Culinary–medicinal mushrooms: A review of organic compounds and bioelements with antioxidant activity. *Eur. Food Res. Technol.* **2021**, *247*, 513–533.
22. Doi, N.; Araki, K.; Fukuta, Y.; Kuwagaito, Y.; Yamauchi, Y.; Sasai, Y.; Kondo, S.; Kuzuya, M. Anti-glycation and antioxidant effects of Chaga mushroom decoction extracted with a fermentation medium. *Food Sci. Technol. Res.* **2023**, *29*, 155–161. [CrossRef]
23. Lawag, I.L.; Nolden, E.S.; Schaper, A.A.M.; Lim, L.Y.; Locher, C. A Modified Folin-Ciocalteu Assay for the Determination of Total Phenolics Content in Honey. *Appl. Sci.* **2023**, *13*, 2135. [CrossRef]
24. Pérez, M.; Dominguez-López, I.; Lamuela-Raventós, R.M. The Chemistry Behind the Folin–Ciocalteu Method for the Estimation of (Poly)phenol Content in Food: Total Phenolic Intake in a Mediterranean Dietary Pattern. *J. Agric. Food Chem.* **2023**, *71*, 17543–17553. [CrossRef] [PubMed]
25. Rizvi, N.B.; Fatima, A.; Busquets, R.; Khan, M.R.; Ashraf, S.; Khan, M.S.; Oz, F. Effect of the Media in the Folin-Ciocalteu Assay for the Analysis of the Total Phenolic Content of Olive Products. *Food Anal. Methods* **2023**, *16*, 1627–1634. [CrossRef]
26. Takatsuka, M.; Goto, S.; Kobayashi, K.; Otsuka, Y.; Shimada, Y. Evaluation of pure antioxidative capacity of antioxidants: ESR spectroscopy of stable radicals by DPPH and ABTS assays with singular value decomposition. *Food Biosci.* **2022**, *48*, 101714. [CrossRef]
27. Rumpf, J.; Burger, R.; Schulze, M. Statistical evaluation of DPPH, ABTS, FRAP, and Folin-Ciocalteu assays to assess the antioxidant capacity of lignins. *Int. J. Biol. Macromol.* **2023**, *233*, 123470. [CrossRef] [PubMed]
28. Kozmelj, T.R.; Voinov, M.A.; Grilc, M.; Smirnov, A.I.; Jasiukaitytė-Grojzdek, E.; Lucia, L.; Likozar, B. Lignin Structural Characterization and Its Antioxidant Potential: A Comparative Evaluation by EPR, UV-Vis Spectroscopy, and DPPH Assays. *Int. J. Mol. Sci.* **2024**, *25*, 9044. [CrossRef] [PubMed]
29. Xie, Z.; Hou, H.; Luo, D.; An, R.; Zhao, Y.; Qiu, C. ROS-Dependent Lipid Peroxidation and Reliant Antioxidant Ferroptosis-Suppressor-Protein 1 in Rheumatoid Arthritis: A Covert Clue for Potential Therapy. *Inflammation* **2021**, *44*, 35–47. [PubMed]
30. Schauen, M.; Hornig-Do, H.T.; Schomberg, S.; Herrmann, G.; Wiesner, R.J. Mitochondrial electron transport chain activity is not involved in ultraviolet A (UVA)-induced cell death. *Free Radic. Biol. Med.* **2007**, *42*, 499–509. [CrossRef] [PubMed]
31. Wang, B.; Wang, Y.; Zhang, J.; Hu, C.; Jiang, J.; Li, Y.; Peng, Z. ROS-induced lipid peroxidation modulates cell death outcome: Mechanisms behind apoptosis, autophagy, and ferroptosis. *Arch. Toxicol.* **2023**, *97*, 1439–1451. [CrossRef] [PubMed]
32. Hong, J.; Lu, H.; Meng, X.; Ryu, J.-H.; Hara, Y.; Yang, C.S. Stability, Cellular Uptake, Biotransformation, and Efflux of Tea Polyphenol (-)-Epigallocatechin-3-Gallate in HT-29 Human Colon Adenocarcinoma Cells. *Cancer Res.* **2002**, *62*, 7241–7246. [PubMed]
33. Karges, J. Reactive Oxygen Species Detection with Fluorescent Probes: Limitations and Recommendations beyond DCFH-DA. *J. Med. Chem.* **2026**, *69*, 1970–1981. [CrossRef] [PubMed]
34. Ruijter, N.; van der Zee, M.; Katsumiti, A.; Boyles, M.; Cassee, F.R.; Braakhuis, H. Improving the dichloro-dihydro-fluorescein (DCFH) assay for the assessment of intracellular reactive oxygen species formation by nanomaterials. *NanoImpact* **2024**, *35*, 100521. [PubMed]
35. Yu, D.; Zha, Y.; Zhong, Z.; Ruan, Y.; Li, Z.; Sun, L.; Hou, S. Improved detection of reactive oxygen species by DCFH-DA: New insight into self-amplification of fluorescence signal by light irradiation. *Sens. Actuators B Chem.* **2021**, *339*, 129878.

36. Lee, S.J.; Kim, J.E.; Choi, Y.J.; Gong, J.E.; Park, S.H.; Douangdeuane, B.; Souliya, O.; Park, J.M.; Lee, H.S.; Kim, B.-H.; et al. Therapeutic Effects of *Dipterocarpus tuberculatus* with High Antioxidative Activity Against UV-Induced Photoaging of NHDF Cells and Nude Mice. *Antioxidants* **2021**, *10*, 791. [CrossRef] [PubMed]
37. Bosch, R.; Philips, N.; Suarez-Perez, J.A.; Juarranz, A.; Devmurari, A.; Chalensouk-Khaosaat, J.; Gonzalez, S. Mechanisms of Photoaging and Cutaneous Photocarcinogenesis, and Photoprotective Strategies with Phytochemicals. *Antioxidants* **2015**, *4*, 248–268. [CrossRef] [PubMed]
38. Hu, X.; Wu, Z.; Zhang, Z.; Yao, H.; Wang, D.-A. Type II collagen scaffolds for tissue engineering. *Commun. Mater.* **2024**, *5*, 149. [CrossRef]
39. Noohi, P.; Mahdavi, S.S.; Abdekhodaie, M.J.; Nekoofar, M.H.; Baradaran-Rafii, A. Photoreactive Hydrogels Based on Type I Collagen Extracted from Different Sources as Scaffolds for Tissue Engineering Applications: A Comparative Study. *Materialia* **2023**, *27*, 101651.
40. Yu, Z.; Smith, M.J.; Siow, R.C.M.; Liu, K.-K. Ageing modulates human dermal fibroblast contractility: Quantification using nano-biomechanical testing. *Biochim. Biophys. Acta (BBA)-Mol. Cell Res.* **2021**, *1868*, 118972. [CrossRef]
41. Krishnan, L.; Weiss, J.A.; Wessman, M.D.; Hoying, J.B. Design and application of a test system for viscoelastic characterization of collagen gels. *Tissue Eng.* **2004**, *10*, 241–252. [CrossRef] [PubMed]
42. Bose, S.; Li, S.; Mele, E.; Silberschmidt, V.V. Dry vs. wet: Properties and performance of collagen films. Part I. Mechanical behaviour and strain-rate effect. *J. Mech. Behav. Biomed. Mater.* **2020**, *111*, 103983. [CrossRef] [PubMed]
43. Wu, C.-C.; Ding, S.-J.; Wang, Y.-H.; Tang, M.-J.; Chang, H.-C. Mechanical properties of collagen gels derived from rats of different ages. *J. Biomater. Sci. Polym. Ed.* **2005**, *16*, 1261–1275. [CrossRef] [PubMed]
44. Rodriguez, R.; Alanis, G.A.; Muñoz, I.A.; Rivera, G.A.; Vargas, S. Detection of hepatic cirrhosis using piezoelectric signals in collagen samples with different ethanol concentrations. *Results Chem.* **2025**, *15*, 102251. [CrossRef]
45. Gopinath, A.; Shanmugam, G.; Madhan, B.; Rao, J.R. Differential behavior of native and denatured collagen in the presence of alcoholic solvents: A gateway to instant structural analysis. *Int. J. Biol. Macromol.* **2017**, *102*, 1156–1165. [CrossRef] [PubMed]
46. Hickman, D.; Sims, T.J.; Miles, C.A.; Bailey, A.J.; de Mari, M.; Koopmans, M. Isinglass/collagen: Denaturation and functionality. *J. Biotechnol.* **2000**, *79*, 245–257. [CrossRef] [PubMed]

Disclaimer/Publisher's Note: The statements, opinions and data contained in all publications are solely those of the individual author(s) and contributor(s) and not of MDPI and/or the editor(s). MDPI and/or the editor(s) disclaim responsibility for any injury to people or property resulting from any ideas, methods, instructions or products referred to in the content.